Modeling of Nanomanipulation with an Integrated Teleoperated System

L. M Fok[1], Y. H. Liu[1], and Wen J. Li[2]

[1]*Networked Sensors and Robotics Laboratory, The Chinese University of Hong Kong*
[2]*Center of Micro and Nano System, The Chinese University of Hong Kong*

***Abstract*—This paper described an integrated system with an Atomic Force Microscope designed for nanomanipulation. Simulation of the nanomanipulation process was accomplished by estimating the interactive forces between molecules of the AFM tip and the sample based on the principle of contact mechanics. The intermolecular force and interactive force between the tip and sample are modeled by the Lennard-Jones potential and the JKR theory, respectively. Besides, stereoscopic visual feedback and force feedback are being provided. This allows user to perform nanomanipulation in a virtual reality environment with force feedback.**

I. Introduction

THE Atomic Force Microscope (AFM) is a system which is designed for investigation of roughness, particle size, or nano scaled surface features [1] – [3]. It can profile samples in real, three-dimensional space with vertical resolution down to 0.1 nm. Because the AFM does not rely on the presence of the tunneling current, a wide range of materials can be used for investigation including semiconductors, non-conducting surfaces, insulators, and biological samples.

The AFM utilizes with a probe which has a microfabrictaed tip mounted on an elastic cantilever to record the attractive and repulsive forces acting between the tip and the sample surface. During operation, the tip is gently in contact with the material and slowly scanned across the surface. The lateral and vertical movements of the tip or sample are controlled by piezoelectric scanners and a feedback loop that produce voltage differences proportional to the movement. The interatomic forces between the atoms on the surface of the material and those on the tip cause the cantilever to deflect. The magnitude of the deflection depends on the separation between the surface atoms and the tip atoms and also the atomic forces between them, such as van der Waals force and adhesion force. The deflection can be recorded by a laser beam focused on the top surface of the cantilever and reflected onto photodetectors as shown in Fig. 1. The detection is made so sensitive that the forces being detected can be as small as a few piconewton. The photodetector signals are used to map the surface topography of samples with resolutions down to the atomic and nano scales.

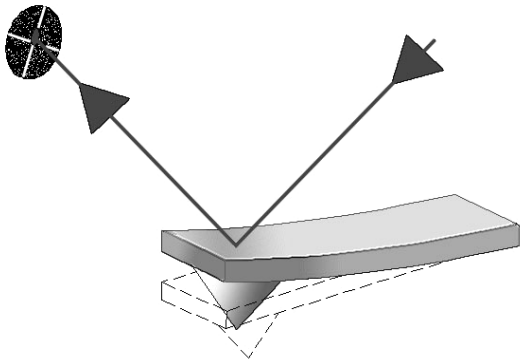

Fig. 1. Detection of the cantilever deflection

There are several techniques that can be employed for fabrication of microstructures such as photolithography [4], microcontact imprint [5], and scanning electrochemical microlithography [6] – [7], but these methods possess significant limitations for patterning structures of nanometer scale. Since the capability to direct pattern polymeric materials at nano-scale creates a number of opportunities, nanolithography has been demonstrated in several systems such as electron beam exposure system [8] and scanning probe microscopes [9] – [10]. Polymer and thin film have been patterned using Scanning Tunneling Microscope (STM) operated in vacuum, as well as using AFM under room conditions. For lithography, the AFM has a distinct advantage over the STM because AFM is used for insulating as well as conducting materials. And patterning by the AFM tip is a non-damaging process with higher precision of alignment and narrower width of lithography than those obtained by the use of photon, electron and scanning probe lithography.

In contact mode, the probe is in contact with the surface and the AFM uses various forces that occur when two objects are brought within nanometers of each other. By indenting the tip onto the sample, patterning on a length scale below 10 nm is realized such as modification of polymer and direct patterning. Varying the magnitude of the applied load can perform either deep scratching or frictionless sliding. There are two ways to vary the applied force which are either by

This work was supported in part by the Hong Kong RGC and the Natural Science Foundation of China under the research grants N-CUHK404/01, CUHK 4199/04E and 60334010

setting the displacement of piezoelectric scanners on defined distance along z axis or tuning the trigger threshold value.

However, AFM-based manipulation is usually not instinctive to the user and requires a high degree of training. With the aid of a force feedback device, direct positioning of the AFM tip with nanometer precision becomes possible. In [11] – [12], systems with direct manipulation are utilized for nanomanipulation. However, direct manipulation is usually slow and imprecise. Closed-loop task-oriented autonomous control was developed in system [13]. In order to avoid problems during operation, it was designed for execution only the given tasks without user interaction. Yet, the automatic control in nanoworld is still challenging due to the complexity of the nanoscale dynamics.

This paper is mainly focused on discussing a teleoperated system with stereoscopic virtual graphical display and haptic force feedback. The graphical user interface was developed from the topography data fed from the AFM, which displayed the surface topography and the position of the AFM tip on the sample. The topography data is scaled to perform the appropriate response on the force feedback joystick and users feel a force proportional to the height of the sample point interacting with the AFM tip. With the aid of the stereoscopic graphical display, users are allowed to perform the nanomanipulation in the virtual nanoworld. The force feedback joystick implemented in the system was a Wingman Force of Logitech with high sensitivity performance, which serves as a haptic interface that provides the users with the sensation of tip-sample interactions. Users are allowed to the control of the whole system by the joystick and switch between navigation and manipulation mode. Scanning by using the AFM is a time consuming process and it was impossible to perform scanning during the manipulation process. In order to estimate the results for the operation, interaction forces between the tip and the sample were being modeled for the simulation. Within the non-contact regime, the tip-sample interaction force is modeled by the Lennard-Jones potential [14] and soon after they are being in contact, the adhesion force is simulated based on the Johnson-Kendall-Roberts (JKR) theory [15].

II. System Architecture

The system architecture of the manipulation system is shown in Fig. 2. The AFM employed for high-resolution imaging is based on a SPM control system (Being Nano-instruments, China), which processes the topographic data and generates the scanning image. Motion of the sample holder is controlled by the piezoelectric actuators in three principal axes.. Two piezoelectric actuators are in plan with the sample, which generate the movement in the x and y directions, and the last one is perpendicular to the sample base, which is responsible for adjusting the separation between the probe tip and the sample. The AFM is capable for nano scale positioning of the sample in 100 μm range in the planar coordinates and 30 μm in the vertical direction. The scanning stage is placed under a light microscope that is equipped with a high-resolution CCD camera for visual control.

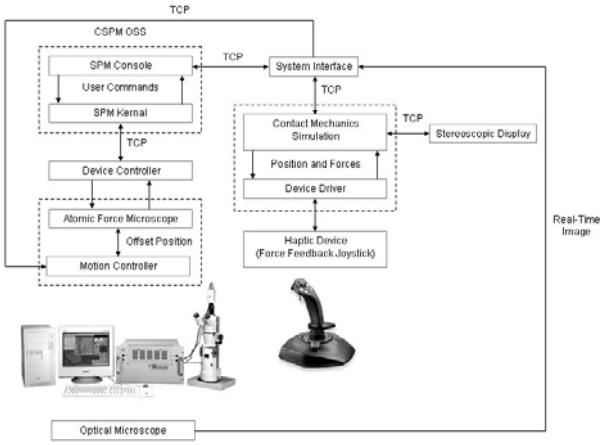

Fig. 2. System architecture of the manipulation system

Real-time image capturing the position of the AFM cantilever is being transferred to the system interface for determination of the distance between the AFM tip and target position. A motion control system equipped with three ultra-resolution electrostrictive actuators and high stability controller (Newport Cooperation, USA) is utilized for automatic local positioning. These are mainly employed for coast positioning of the sample and their resolution is 0.1 μm The motion of the motion control system mainly depends on the calculated distance between the probe tip and the location under investigation.

Tracing the deflection as a function of the piezo position yields a force-displacement curve, which resembles a hystersis loop that exemplifies the operation of the AFM, for the calculation of contact force. On the other hand, it also represents the change of state of the cantilever during scanning. This curve is used to characterize features that can be used to determine interaction forces and mechanical properties. In a typical force curve as shown in Fig. 4, the vertical axis of the graph represents the cantilever deflection signal which is the difference in voltage signals produced by the upper and lower photodetectors in the optical head. The voltage applied to the z piezoelectric scanner is plotting along the horizontal axis. The force curve represents the deflection signal for one complete extension or retraction cycle of the piezoelectric scanner.

III. Interatomic Forces

The interaction between the tip and sample of an atomic force microscope consists of a variety of forces such as electric, magnetic, and atomic forces for the non-contact regime and indentation, adhesion, and capillary forces for the contact regime.

A. Indentation and Adhesion Forces

The tip and sample are modeled as two spheres [15] as illustrated in Fig. 3. Consider the contact of a sphere of radius R_t with elastic modulus of E_t and Poison's ratio ν_t with the sample surface of radius R_s, elastic modulus of E_s, and Poison's ratio of ν_s. If there is no pressure applied between them, the contact occurs only at the point O if in the absence of surface energy. If one sphere is forced down by a load F, the centers of the two spheres approach by a quantity δ, and the contact is achieved on a circle of radius r. It is assumed that the ratio of r/R_t and r/R_s are both small, no friction occurs at the interface and no tensile stress exists in area of contact.

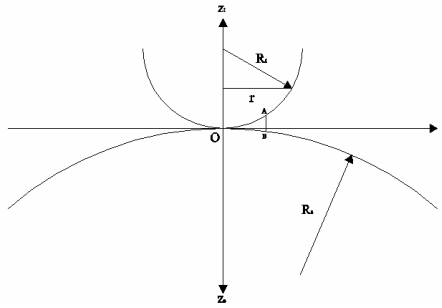

Fig. 3. Two spheres in contact at a point

The equations of the two circles are given by,

$$r^2 + (z_t - R_t)^2 = R_t^2 \tag{1}$$

$$r^2 + (z_s - R_s)^2 = R_s^2 \tag{2}$$

The distance between A and B near O is expressed as a function of the radial distance r

$$AB = \frac{r^2}{2R} = h \tag{3}$$

which the distance between the probe tip and the sample surface as shown in Fig. 4 and R is the effective tip-sample radius of curvature

$$\frac{1}{R} = \frac{1}{R_t} + \frac{1}{R_s} \tag{4}$$

When a load is applied to the tip in contact with a surface such that the point at which load is applied moves a vertical distance δ. If this distance is measured with respect to a distant point on the surface, this may be considered as the distance of mutual approach between the tip and the surface. In general both the tip and surface undergo deformation. If the tip is rigid, there will be no deformation.

The adherence force between two elastic spheres could be measured by the Johnson, Kendall and Roberts (JKR) theory. In the presence of surface energy, the contact area sustains infinite stress on its periphery. It remains finite under negative loads until a critical traction force is reached at which the surfaces separate abruptly. The surface energy, γ required to separate two flat surfaces from contact to infinity is defined as,

$$\gamma = \frac{H}{24\pi D_0^2} = \frac{W_{1,2}}{2} \tag{5}$$

where H is the Hamaker's constant, $D_0 \left(= \sigma / 2.5\right)$, $\sigma = 0.4125nm$ is the typical interatomic distance, and $W_{1,2}$ is the work of adhesion.

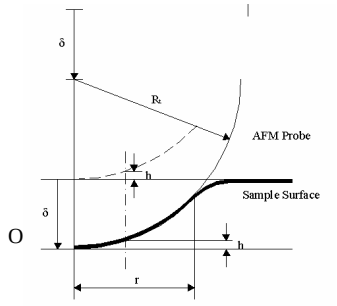

Fig. 4. Contact between two elastic spheres

The elastic modules of the two spheres are modeled as

$$\kappa_t = \frac{1-\nu_t^2}{\pi E_t} \tag{6}$$

and

$$\kappa_s = \frac{1-\nu_s^2}{\pi E_s} \tag{7}$$

The effective elastic modulus, κ, is then expressed as

$$\kappa = \kappa_t + \kappa_s \tag{8}$$

According to the JKR Theory, the tip-sample contact forces as a function of the contact radius is

$$F = \frac{Kr^3}{R} - \sqrt{\frac{2Kqr^3}{R}}, \tag{9}$$

where $K = \frac{4}{3\pi\kappa}$, and $q = 3\pi R W_{1,2}$.

The indentation, δ, as a function of the applied force is

$$\delta = \frac{r^2}{3R} + \frac{2F}{3rK}. \tag{10}$$

Lennard-Jones Forces

Denote the initial position of the AFM cantilever by u and the displacement of the tip by s. The deflection of the cantilever, d, is described as $d = s - u$. The deflection of the cantilever is expressed as a function of the piezo displacement. The Lennard-Jones potential, W, is used for modeling of interactive forces in non-contact regime and is given by

$$W = \left[\frac{HR_t}{6\sigma}\right]\left[\frac{1}{210}\left(\frac{\sigma}{s}\right)^7 - \frac{\sigma}{s}\right]. \quad (11)$$

The Lennard-Jones force, F_L, is obtained from the potential by taking the negative of its derivative with respect to s.

$$F_L = \frac{HR_t\left(-30s^6 + \sigma^6\right)}{180\,s^8}. \quad (12)$$

The deflection of the cantilever as a function of the piezo displacement is expressed as

$$d(s) = \frac{F_L(s)}{k}, \quad (13)$$

where k is the spring constant of the cantilever.

The tip jumps to contact with the surface (snap-in) or pulls out of the surface (pull-out) when the derivative of the force equals to the spring constant. The values of snap-in and pull-out point are obtained by solving

$$\frac{dF_L}{ds} = k. \quad (14)$$

IV. Nanomanipulation

In the experiment, the AFM is employed as a tool for nanolithography by controlled tip motion on various material surfaces. Nanolithography may be used to investigate various material properties and this could be conducted within the area bounded by the maximum scan size. The deflection of the cantilever accomplishes as a measure of the force.

The trigger threshold is the value of the cantilever deflection, as measured by the photodetectors, desired for the indentation or lithography. It defines the maximum force applied to the sample corresponding to the upper leftmost point on the force plot as shown in Fig. 5. During each step, the tip is pushed into the sample surface until the cantilever deflection equals the trigger threshold. At this point, the tip is either lifted up away from the sample to remove the load, if indenting, or the tip is moved laterally in a prescribed direction, if scratching. The cantilever deflection is measured relative to the value of the deflection at the surface contact point, located somewhere on the flat portion of the force plot where the force is zero.

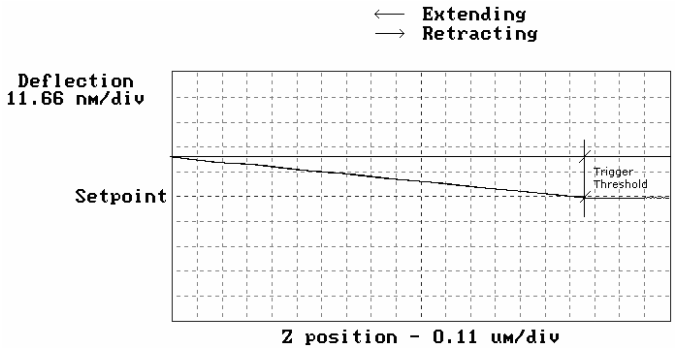

Fig. 5. Trigger threshold shows in the force plot

The cantilever sensitivity is the cantilever deflection signal versus the voltage applied to the z piezo determined from the slope of the force plot. The sensitivity of the cantilever must be measured in order to calculate the force applied to the sample during indentation. Once the sensitivity is known, the force, F_z, of indentation is determined from Hooke's Law,

$$F_z = k \times x = k \times V_t . \times s \quad (15)$$

where x is the cantilever deflection in nm, V_t is the trigger threshold voltage, and s is the cantilever sensitivity in nm/V. The cantilever deflection is determined from the cantilever sensitivity and the maximum deflection used for the indentation.

V. Experiments and Discussions

The graphical interface was developed based on the topographic data obtained from the AFM. The 3D surface was generated according to the height data and users are allowed to perform navigation of the surface in a virtual reality environment. Besides, users can execute lithography on the surface in manipulation mode, Fig. 6(a) and 6(b) show the surface before and after simulation, respectively. The depth of indentation is estimated by the JKR theory.

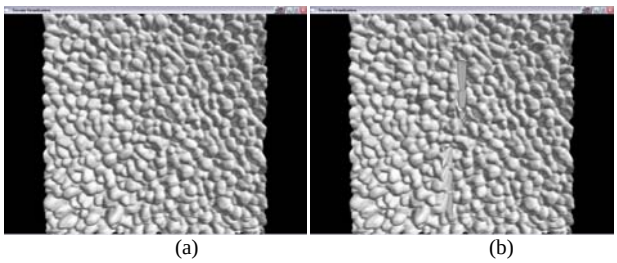

(a) (b)

Fig. 6. Stereoscopic interface for navigation and manipulation

During operation, when the distance between the tip position and the sample surface is below the range of 100 *nm*, the interaction force is being simulated and it is used to estimate the results for the manipulation. Prior to the simulation, users are allowed to modify the setting of parameters. The depth of indentation is estimated by the

applied force of the user. According to the parameters defined in Table 1, the depth of lithography with applied force of 1.5 μN was 5.9 *nm*. Fig. 9 illustrates that the depth of indentation increased with increasing applied load.

TABLE I
SETTING OF PARAMETERS FOR SIMULATION

Parameters	Value
Tip radius	30 *nm*
Sample radius	100 *nm*
Young's modulus of Au	$0.08\times10^{12}\ N/m^2$
Young's modulus of Polymer	$0.001\times10^{12}\ N/m^2$
Poisson ratio of Au	0.42
Poisson ratio of Polymer	0.3
Hamaker's constant of Au	$45.5\times10^{-20}\ J$
Hamaker's constant of Polymer	$6.2\times10^{-20}\ J$

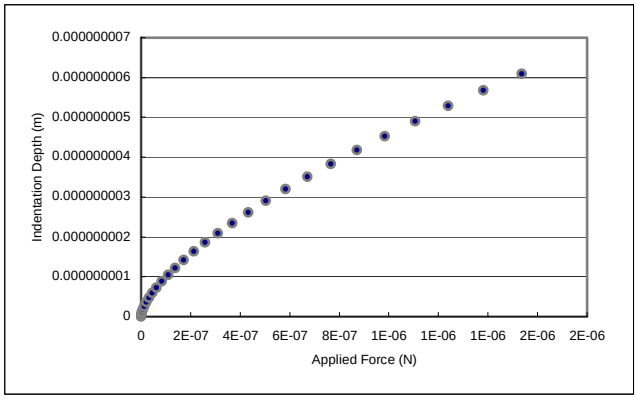

Fig. 7. The depth of indentation as a function of the applied force

In order to verify the model, the simulation results are being compared to the experimental results. The AFM cantilever used for this study is a silicon nitrate cantilever of tip radius 30 *nm*, and stiffness of 0.6 *N/m*. All measurements were performed in an ambient environment. The Parylene thin film was produced by deposition of Parylene C on Si (100) wafers, which was about 0.3 μm thick. Samples were scanned orthogonal to the long axis of the cantilever with average load 1.5 μN to generate scratches. Observations of the sample surface before and after the scratch tests were done by scanning parallel to the long axis of the cantilever with loads of 0.2 μN as the parallel scans enable minimum wear of the sample surface. In the scratch test, scratches are generated in a replicate mode at a given load for 1, 2 and 3 cycles over a scan length of 5 μm at 5 $\mu m/s$. The 2D and 3D scanned image after the scratch test were as shown in Fig. 8 and Fig. 9, respectively.

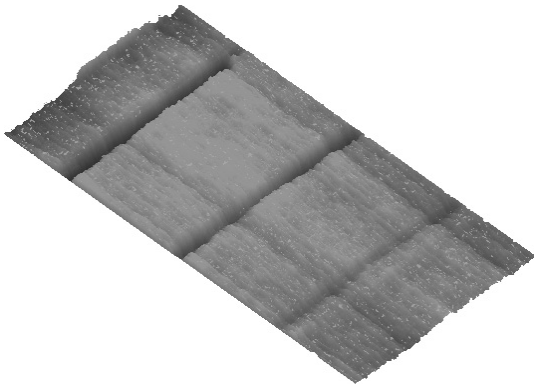

Fig. 8. 3D image of lithography on Parlyene C

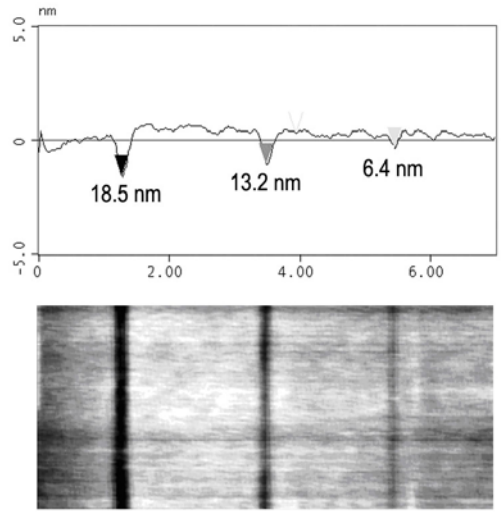

Fig. 9. 2D topographic image and 2D sections after lithography

When applied one cycle of scratch, the depth of the channel is 6.4 *nm*, the depths for 2 cycles and 3 cycles are 13.2 *nm* and 18.5 *nm*, respectively. It was found that with constant applied load, the depth and width increases almost linearly with increasing number of cycles. This suggested that the material was removed layer by layer during the test. Comparing the experimental results with the simulation results, the difference is about 0.5 *nm* and this may due to the capillary force appear on the sample surface.

This technique was applied to channels fabrication between gold electrodes on silicon substrate. Fig. 10(a) and Fig. 10(b) show the topography of the device before and after nanolithography, respectively. The width and the maximum depth are about 8 *nm* and 15 *nm*, respectively. The depth of the channel varied with the number of cycle of scratch. The widths of the electrodes are about 5 μm and it is difficult to fabricate a channel between them using traditional lithography technique. On the other hand, the AFM based nanolithography guarantees for precision in localization and this could be applied for the fabrication of nano channels..

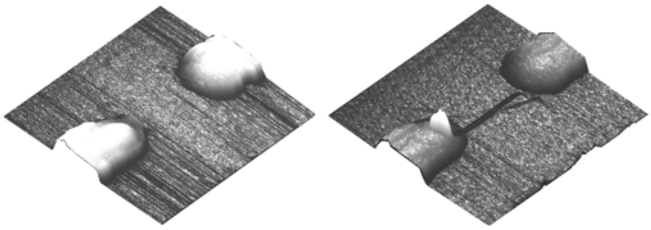

(a) (b)

Fig. 10. Lithography of a channel between gold electrodes on silicon surface

VI. CONCLUSION

This paper describes a haptic interface developed for nanomanipulation with the AFM, which allows the user to act on and feel the nanoworld phenomena through navigation and manipulation. The manipulation process is being simulation based on the contact mechanics during the manipulation process. The Lennard-Jones potential is employed to model of tip-sample interaction forces when the AFM tip and material surface are in contact. Indentation and adhesion forces are modeled from JKR theory for contact regime. The motion behaviors of the AFM cantilever and relations between the applied force and depth of indentation have been analyzed. These experimental results provide insight into the mechanics of an AFM-based nanolithography. A model for frictions will be implemented in the future so that manipulation by the use of force feeling will become more accurate and predictable.

Nanolithography with contact mode imaging technique has been shown to be a powerful tool. Scratches of various depths and widths were produced and controlled by the number of cycles. An advantage of using AFM for nanolithography over other instruments is that precise localization could be performed based on the high resolution image obtained.

REFERENCES

[1] J. Mou, D. M. Czajkowsky, S. J. Sheng, R. Ho, and Z. Shao, "High resolution surface structure of E. coli GroeS Oligomer by Atomic Force Microscopy," *FEBS Letters*, vol. 381, pp.161 – 164, 1996.

[2] Y. E. Strausser, M. Schroth, and J. J. Sweeney, "Characterization of the low-pressure chemical vapor deposition grown rugged polysilicon surface using atomic force microscopy," *J. Vas. Sci. Technol. A*, vol. 15, pp. 1007, 1997.

[3] W. Fritzsche, L. Takac, and E. Henderson, "Application of atomic force microscopy to visualization of DNA, chromatin, and chromosomes," *Critical Reviews in Eukaryotic Gene Expression*, vol. 7, pp. 231 – 240, 1997.

[4] S. Roth, L. Dellmann, G. A. Racine, and N. F. de Rooij, "High aspect ratio UV photolithography for electroplated structures," *J. Micromech. Mecroeng.*, vol. 9, pp. 105 – 108, 1999.

[5] E. Kim, G. M. Whitesides, M. B. Freiler, M. Levy, J. L. Lin, and R. M. Osgood Jr., "Fabrication of micrometer-scale structures on GaAs and GaAs/AlGaAs quantum well material using microcontact printing," *Nanotechnology*, vol. 7, pp. 266 – 269, 1996.

[6] H. Ohji, P. T. J. Gennissen, P. J. French, and K. Tsutsumi, "Fabrication of a beam-mass structure using single-step electrochemical etching for micro structures (SEEMS)," *J. Micromech. Microeng.*, vol. 10, pp. 440 – 444, 2000.

[7] R. A. Said, "Microfabrication by localized electrochemical deposition: experimental investigation and theoretical modeling," *Nanotechnology*, vol. 15, pp. 867, 2004.

[8] H. Iwasaki, T. Yoshinobu, and K. Sudoh, "Nanolithography on SiO_2/Si with a scanning tunneling microscope," *Nanotechnology*, vol. 14, pp. 55 - 62, 2003.

[9] A. Majumdar, P. I. Oden, J. P. Carrejo, L. A. Nagahara, J. J. Graham, and J. Alexander, "Nanometer-scale lithography using the atomic force microscope," *Applied Physics Letters*, vol. 61, pp. 2293-2295, 1992.

[10] C. K. Hyon, S. C. Choi, S. H. Song, S. W. Hwang, M. H. Son, D. Ahn, Y. J. Park, and E. K. Kim, "Application of atomic-force-microscope direct patterning to selective positioning of InAs quantum dots on GaAs," *Applied Physics Letters*, vol. 77, pp. 2607 – 2609, 2000.

[11] M. Falvo, R. Superfine, S. Washburn, M. Finch, R. M. Taylor, V. L. Chi, and F. P. Brooks Jr.., "The nanomanipulator: A teleoperator for manipulating materials at the nanomerter scale," *Proc. of Int. Symp. On Science and Technology of Atomically Engineered Materials*, pp. 579 – 586, 1996.

[12] M. Sitti, and H. Hashimoto, "Tele-nanorobotics using atomic force microscope as a robot and sensor," *Advanced Robotics Journal*, vol. 13, no. 4, pp. 417 – 436, 1999.

[13] M. Sitti, and H. Hashimoto, "Two-dimensional fine particle positioning under optical microscope using a piezoresistive cantilever as a manipulator," *Journal of Micromechatronics*, vol. 1, no. 1, pp. 25 – 48, 2000.

[14] P. L. Huyskens, W. A. P. Luck, and T. Z. Huyskens, *Intermolecular Force, An Introduction to Modern Methods and Results*, Spring-Verlag, Berlin, Heidelbery, 1991.

[15] J. Israelachvili, *Intermolecular and Surface Force*, Academic Press, 2nd edition, 1991